Laser Phys. Lett. **4**, No. 9, 660–667 (2007) / **DOI** 10.1002/lapl.200710048

Abstract: High-order stimulated Raman scattering (SRS) and cascaded $\chi^{(3)} \rightarrow \chi^{(2)}$ generation effects in new nonlinear-laser crystals of PbB_4O_7 were observed with picosecond laser pumping. All registered $\chi^{(3)}$- and $\chi^{(2)}$-lasing components in the visible and near-IR were identified and attributed to the SRS-promoting mode $\omega_{SRS} \approx 148$ cm^{-1} of the studied crystal.

Example of a grown crystal of PbB_4O_7, together with two crystal samples that were cut from the bulk of the crystal

High-order stimulated Raman scattering and cascaded nonlinear lasing effects in crystals of ($\chi^{(3)} \rightarrow \chi^{(2)}$)-active orthorhombic PbB_4O_7

A.A. Kaminskii, [1,*] *L. Bohatý,* [2] *P. Becker,* [2] *J. Liebertz,* [2] *L. Bayarjargal,* [2] *J. Hanuza,* [3,4] *H.J. Eichler,* [5] *H. Rhee,* [5] *and J. Dong* [6]

[1] Institute of Crystallography, Russian Academy of Sciences, Moscow 119333, Russia
[2] Institute of Crystallography, University of Cologne, 50674 Cologne, Germany
[3] Institute of Low Temperature and Structure Research, Polish Academy of Sciences, 50950 Wrocław, Poland
[4] Department of Bioorganic Chemistry, Institute of Chemistry and Food Technology, 50345 Wrocław University of Economics, Wrocław, Poland
[5] Institute of Optics and Atomic Physics, Technical University of Berlin, 10623 Berlin, Germany
[6] Institute for Laser Science, University of Electro-Communications, 182-8585 Tokyo, Japan

Received: 25 April 2007, Accepted: 28 April 2007
Published online: 4 May 2007

Key words: stimulated Raman scattering; Raman borate crystal; PbB_4O_7; lead tetraborate; nonlinear laser cascading; Stokes and anti-Stokes generation; Raman laser converters

PACS: 78.30.-j, 42.65.Dr, 42.65.Ky, 42.55.Rz

1. Introduction

Borate crystals nowadays are a well-established family of active materials for laser frequency doublers and stimulated Raman scattering (SRS) frequency converters, that base either on $\chi^{(2)}$ and $\chi^{(3)}$ nonlinearities or cascaded $\chi^{(3)} \leftrightarrow \chi^{(2)}$ processes, as well as for solid-state lasers, that can generate stimulated emission (SE) of their trivalent lanthanide (Ln^{3+}) activators (see Table 1 and [1,2]). Among them the nonlinear-laser crystal PbB_4O_7 is a member of the isomorphic series of polar orthorhombic tetraborates $M^{II}B_4O_7$ (with M^{II} = Pb [3], Sr [4], Eu [5], Ca (high pressure) [6], Hg (high pressure) [7], and Sn (high-pressure) [8]) and had been subject to investigations of nonlinear optical properties already in the eighties. With its electro-optic constants PbB_4O_7 ranges among the known borates with highest value of this property [9].

Recently, lead tetraborate was found to possess the highest value of tensor coefficients of second harmonic generation (SHG) d_{ijk}^{SHG} among all non-centrosymmetric borates investigated so far [10]. Unfortunately, as it was already stated also by [11], the refractive indices of PbB_4O_7 do not allow the realization of phase matching conditions for second harmonic generation (SHG). In this letter, we

* Corresponding author: e-mail: kaminalex@mail.ru

Crystal	Space group	SE[a)]	SHG	THG[b)]	SRS	Self-FG (SE)[c)]	Self-FD (SRS)[d)]	Self-SRS (SE)[e)]	Self-SRS (SHG)[f)]	Self-SFM[g)]	Self-DFH[h)]	OPO[i)]
Monoclinic crystals												
$Ca_4Y(BO_3)_3O$	C_s^3	+	+		+	+		+				
$Ca_4Gd(BO_3)_3O$	C_s^3	+	+		+							
$Sr_4Y(BO_3)_3O$	C_s^3	+										
$La_2CaB_{10}O_{19}$	C_2^3	+	+			+						
BiB_3O_6	C_2^3	[j)]	+	+(?)	+	+(?)			+	+		+
Orthorhombic crystals												
LiB_3O_5	C_{2v}^9		+									
$K_3Nb_3O_6(BO_3)_2$	C_{2v}^2		+		+							
CsB_3O_5	D_2^4		+	+(?)								
PbB_4O_7	C_{2v}^7		+[k)]		+					+		
Tetragonal crystals												
$Li_2B_4O_7$	C_{4v}^{12}		+[l,m)]	+[l)]	+		+		+	+		
$LiGeBO_4$	S_4^2				+		+[k)]					
$CsLiB_6O_{10}$	D_{2d}^{12}		+									
Trigonal crystals												
$\beta-YAl_3(BO_3)_4$	D_3^7	+	+			+						
$\beta-BaB_2O_4$	C_{3v}^6	[j)]	+[m)]	+	+				+	+[n)]		+
$\beta-LaBGeO_5$	C_3^2	+	+[o)]		+	+	+	+	+	+	+	
$\beta-LaSc_3(BO_3)_4$	D_3^7	+	+			+						
$\beta-CeSc_3(BO_3)_4$	D_3^7	+	+			+						
$\beta-GdAl_3(BO_3)_4$	D_3^7	+	+			+				+		
Hexagonal crystal												
$BaCaBO_3F$	D_{3h}^3	+	+(?)									

[a)] Presently, in these boron containing non-centrosymmetric crystals SE was obtained with four Ln^{3+} lasants: Pr^{3+}, Nd^{3+}, Er^{3+}, and Yb^{3+}.
[b)] THG: third harmonic generation.
[c)] Self-FD(SE): self-frequency doubling, i.e., cascaded SHG from arising SE in Ln^{3+}-ion doped crystals with non-laser and laser pumping.
[d)] Self-FD(SRS): self-frequency doubling, i.e., cascaded SHG from arising Stokes and anti-Stokes generation in undoped crystals with external laser excitation.
[e)] Self-SRS(SE): self-stimulated Raman scattering, i.e., cascaded laser Raman Stokes and anti-Stokes generation by the action of arising SE in Ln^{3+}-ion doped crystals with external laser radiation.
[f)] Self-SRS(SHG): self-stimulated Raman scattering, i.e., cascaded laser Raman Stokes and anti-Stokes generation by the action of arising SHG in undoped crystals with external laser radiation.
[g)] Self-SFM: self-sum-frequency mixing, i.e., cascaded summing parametric generation (up-conversion processes) between arising secondary laser emissions (e.g., SE, SRS, SHG, and others), as well as laser excitation radiation in Ln^{3+}-ion doped and undoped crystals with external non-laser and laser pumping.
[h)] Self-DFG: self-difference-frequency generation, i.e., cascaded difference parametric interaction (down-conversion processes) between arising secondary laser emissions and laser pumping radiation.
[i)] OPO: optical parametric oscillation.
[j)] Can be activated by Ln^{3+} lasants.
[k)] Non phase-matchable frequency doubling in the visible.
[l)] Cherenkov-type SHG and THG were observed as well.
[m)] It is possible also the collinear fourth harmonic generation with birefringent phase-matching.
[n)] Also, self-sum-frequency generation in an optical parametric amplifier by mixing between the pumping and arising idler wavelengths.
[o)] Cherenkov-type SHG was observed as well.

Table 1 Selected laser and non-centrosymmetric nonlinear-laser borate crystals and their $\chi^{(2)}$-, $\chi^{(3)}$-, and cascaded ($\chi^{(3)} \leftrightarrow \chi^{(2)}$)-frequency conversion and lasing effects

report on the first observation of high-order Raman Stokes and anti-Stokes generation and cascaded ($\chi^{(3)} \rightarrow \chi^{(2)}$)-lasing effects in PbB_4O_7 single crystals with picosecond one-micron laser excitation.

2. Crystallography

The crystal structure of PbB_4O_7 (that was already mentioned to be isomorphous to SrB_4O_7 by [3]) was first determined by [11]. A detailed structure investigation with an emphasis on the influence of the stereochemical active lone electron pair of Pb^{2+} was recently presented by [12]. PbB_4O_7 crystallizes in the non-centrosymmetric, polar space group $Pnm2_1$ with a_1 = 4.4535(4) Å, a_2 = 10.8346(9) Å, and a_3 = 4.2441(3) Å [12] (see also footnote [b)] in Table 2). The crystal structure consists of exclusively four-fold (tetrahedrally) coordinated boron atoms and lead atoms with an irregular oxygen coordination of which the coordination number is not clearly defined. Setting a cut-

Characteristic				
Space group [3]	$C_{2v}^7 - Pnm2_1$ (No. 31) [b]			
Unit cell parameters, Å [12]	a_1 = 4.4535(4) (= a); a_2 = 10.8346(9) (= b); a_3 = 4.2441(3) (= c)			
Formula units per unit cell [3]	Z = 2			
Fractional coordinates, site symmetry (*ss*) and coordination number (*CN*) of atoms [12]	x	y	z	ss
	Pb: 0.69835(1)	0	0	$m(C_s)$
	CN = 10 [c]			
	B1: 0.8258(2)	0.3779(1)	0.0067(9)	$1(C_1)$
	CN = 4			
	B2: 0.3230(3)	0.2483(1)	0.0345(5)	$1(C_1)$
	CN = 4			
	O1: 0.2657(3)	0	0.6140(4)	$m(C_s)$
	O2: 0.1400(2)	0.3561(1)	0.0822(3)	$1(C_1)$
	O3: 0.7701(2)	0.3637(1)	0.6745(3)	$1(C_1)$
	O4: 0.3709(2)	0.2200(1)	0.6799(2)	$1(C_1)$
Density, g cm^{-3} [11,12]	$d_x \approx 5.88$			
Melting temperature, K [13]	$T_m \approx 1047$			
Method of crystal growth	top-seeding technique [14,15], modified Czochralski [15–17]			
Linear optical character	biaxial negative ($n_1^0 \gtrsim n_3^0 > n_2^0$)			
Optical transparency range, μm [d]	$\approx$ 0.23 – $\approx$ 3.2 (see also Fig. 3)			
Refractive index (modified Sellmeier equation) [10] [e]	$n^2(\lambda) = D_1 + \frac{D_2}{(\lambda^2 - D_3)} - D_4\lambda^2$ (see also Fig. 3)			
Nonlinearity	$\chi^{(2)}$ and $\chi^{(3)}$			
Nonlinear optical susceptibilities, 10^{-12} m V^{-1} [10] [f]	$d_{311}^{SHG} = 2.3(3)$; $d_{322}^{SHG} = 2.8(5)$; $d_{333}^{SHG} = 4.0(4)$; $d_{113}^{SHG} = 0.68(5)$; $d_{223}^{SHG} = 0.57(5)$			
Phase matching condition for SHG	not phase-matchable in the entire transparency range			
Linear electro-optic coefficients at constant stress, 10^{-12} m V^{-1} [9] [g]	$r_{113}^{\sigma} = 2.35(8)$; $r_{223}^{\sigma} = 2.40(8)$; $r_{333}^{\sigma} = 2.83(9)$; $r_{131}^{\sigma} = 0.68(5)$; $r_{232}^{\sigma} 0.95(7)$			
Piezoelectric (linear electrostrictive) coefficients, 10^{-12} m V^{-1} [9] [h]	$d_{311} = 2.8(2)$; $d_{322} = 2.6(2)$; $d_{333} = \pm 0.0(1)$; $d_{113} = 2.1(1)$; $d_{223} = 1.7(2)$			
Pyroelectric coefficient at constant stress and its temperature dependence, [i] 10^{-6} C m^{-2} K^{-1} [18]	$p_3^{\sigma}(T) = 19.81 - 2.741 \times 10^{-2}T + 2.924 \times 10^{-5}T^2$ (standard deviation: 0.4)			
Phonon spectrum extension, cm^{-1} [j]	≈ 1100			
Energy of SRS-promoting vibration mode, cm^{-1}	$\omega_{SRS} \approx 148$ (see also Fig. 4)			
Width of Raman shifted line related to SRS-promoting vibration transition, cm^{-1}	$\Delta\nu_R \approx 6$ cm^{-1} (see also Fig. 5a)			
Possible applications	UV/VIS electro-optic Q-switchers/modulators, surface acoustic wave devices [15], Raman laser converters			

[a] Limit of probable error in parentheses.
[b] Original data from [12] that are given in standard setting *Pmn*2$_1$ were transformed to the non-standard setting *Pnm*2$_1$, that had already been used for all previous physical investigations. Note that in [3] and [11] a non-standard setting $P2_1nm$ is used.
[c] Using a cut-off value for the nearest neighbours of 3.1 Å.
[d] For $\approx$ 1.7-mm thick (100)-plate.
[e] Sellmeier coefficients: λ is in μm, (the refractive indices were determined in the wavelength range 0.365 – 1.083 μm using the prism method and corrected with the refractive index of air; ξ^2 is the sum of the squares of the residuals). See also [16,17].

	D_1	D_2	D_3	D_4	ξ^2
n_1^0	3.644911	0.036662	0.0272	0.022440	0.1×10^{-8}
n_2^0	3.625194	0.035386	0.0265	0.024742	0.5×10^{-8}
n_3^0	3.638438	0.036738	0.0271	0.021697	4.8×10^{-8}

[f] For λ = 1.064 μm wavelength.
[g] For λ = 0.6328 μm wavelength.
[h] Further published data of piezoelectric constants (as well as elastic and dielectric constants) by [19] were not included due to inconsistencies and severe confusions in these publications.
[i] Within temperature range 163 – 400 K.
[j] From spontaneous Raman scattering spectra.

Table 2 Crystallographic and some physical properties of orthorhombic PbB_4O_7 single crystals at room temperature (unless indicated otherwise) [a]

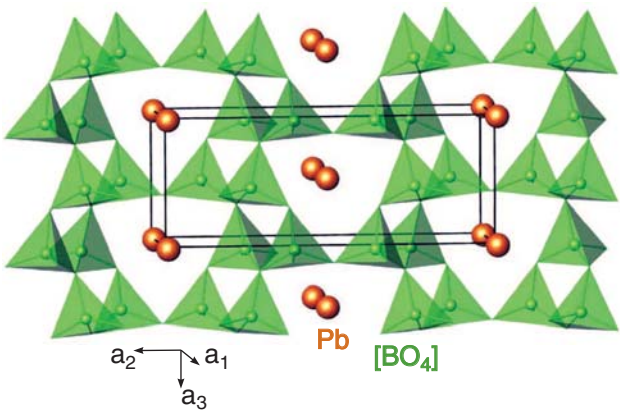

Figure 1 (online color at www.lphys.org) Plot of the crystal structure of PbB_4O_7. $[BO_4]$ groups are marked with green tetrahedra, Pb is marked with large orange spheres. Pb atoms are located in tubular voids of the borate network that run along a_1 and a_3. (Data taken from [12])

Figure 2 (online color at www.lphys.org) Example of a grown crystal of PbB_4O_7, together with two crystal samples that were cut from the bulk of the crystal

off value for the nearest neighbour distances at 3.1 Å lead is 10-fold coordinated with oxygen (the distance between Pb and the next nearest cation, boron, is 3.17 Å). The $[BO_4]$ borate units are linked via common oxygen atoms to a three-dimensional network with tubular voids, where the lead atoms are situated, that run parallel to the a_1 and the a_3 axis of the structure, see Fig. 1. Lead as well as one of the oxygen atoms (O1) are in a special position

Stokes and anti-Stokes lasing components		
Wavelength, μm [a)]	Line	SRS- and RFWM-line attribution [b)]
0.5279	SFM	$\omega_f + \omega_{ASt1}(\omega_f + \omega_{SRS})$
0.53207	SHG(λ_f/2)	$2\omega_f$
0.5363	SFM	$\omega_f + \omega_{St1}(\omega_f - \omega_{SRS})$
0.5406	SFM	$\omega_f + \omega_{St2}(\omega_f - 2\omega_{SRS})$
0.5450	SFM	$\omega_f + \omega_{St3}(\omega_f - 3\omega_{SRS})$
0.8719	ASt_{14}	$\omega_f + 14\omega_{SRS}$
0.8833	ASt_{13}	$\omega_f + 13\omega_{SRS}$
0.8950	ASt_{12}	$\omega_f + 12\omega_{SRS}$
0.9070	ASt_{11}	$\omega_f + 11\omega_{SRS}$
0.9194	ASt_{10}	$\omega_f + 10\omega_{SRS}$
0.9320	ASt_9	$\omega_f + 9\omega_{SRS}$
0.9451	ASt_8	$\omega_f + 8\omega_{SRS}$
0.9585	ASt_7	$\omega_f + 7\omega_{SRS}$
0.9723	ASt_6	$\omega_f + 6\omega_{SRS}$
0.9865	ASt_5	$\omega_f + 5\omega_{SRS}$
1.0011	ASt_4	$\omega_f + 4\omega_{SRS}$
1.0162	ASt_3	$\omega_f + 3\omega_{SRS}$
1.0317	ASt_2	$\omega_f + 2\omega_{SRS}$
1.0477	ASt_1	$\omega_f + \omega_{SRS}$
1.06415	λ_f	ω_f
1.0812	St_1	$\omega_f - \omega_{SRS}$
1.0988	St_2	$\omega_f - 2\omega_{SRS}$
1.1169	St_3	$\omega_f - 3\omega_{SRS}$
1.1357	St_4	$\omega_f - 4\omega_{SRS}$
1.1551	St_5	$\omega_f - 5\omega_{SRS}$
1.1752	St_6	$\omega_f - 6\omega_{SRS}$

[a)] Measurement accuracy is ± 0.0003 μm.
[b)] $\omega_{SRS} \approx 148$ cm^{-1}.

Table 3 Room-temperature spectral composition of Stokes and anti-Stokes generation in orthorhombic PbB_4O_7 single crystals with picosecond Nd^{3+}:$Y_3Al_5O_{12}$-laser pumping at $\lambda_f = 1.06415$ μm wavelength under excitation geometry $c(qq)c$ (with $\mathbf{q} \parallel (\mathbf{e}_1 + \mathbf{e}_2)$

with site symmetry m, all other atoms are in general position with site symmetry 1. Since PbB_4O_7 melts congruently [13] in principle single crystals can be grown from a melt of stoichiometric composition. However, due to the rather high viscosity of the melt a slight excess of PbO, that reduces the viscosity to some extend, proved to be advantageous. The crystals used in our study were grown in our laboratory by the top seeding technique without crystal pulling or rotation, as it has been described already in [14]. The crystals were of high optical quality with dimensions up to $20\times28\times55$ mm^3. Fig. 2 gives an example of a grown crystal together with samples cut from the bulk. For the investigation and description of all physical properties a Cartesian reference system $\{\mathbf{e}_i\}$ with $\mathbf{e}_i \parallel \mathbf{a}_i$ ("crystalphysical system") is used. The positive direction of the polar diad a_3-axis is defined by the positive sign of the transverse piezoelectric coefficient d_{311} (or d_{322}). Our SRS measurements were performed on two crystal samples with different orientations that were cut and prepared

Vibrational mode wave numbers, cm^{-1}		Assignment [b]
$c(bb)c$ [a] A_1-TO (see Fig. 4b)	$c(aa)c$ [a] A_1-LO (see Fig. 4a)	
89 w 103 m 121 vw 148 vs	92 vw 105 w 121 w 148 vs	T′ (Pb^{2+}, B^{3+})
248 s 261 m 273 vw	 262 m 273 m	δ(BOB)
293 s 353 vs	293 vw 353 vs	$\delta_s(BO_4) - \nu_2$
410 w	410 w 420 w 433 vw	$\delta_{as}(BO_4) - \nu_4$+ T′($B^{3+}$)
485 s	485 s 504 vw	ν_s(BOB) + T′(B^{3+})
527 vw 545 vw 564 w	527 vw 564 s 623 s	$\nu_s(BO_4) - \nu_1$
 841 m	697 m	ν_{as}(BOB)
 948 vw 1008 vw 1093 s	907 vw 1007 s 1087 vw	$\nu_{as}(BO_4) - \nu_4$

[a] Here: vw – very weak, w – weak, m – medium, s – strong, vs – very strong.
[b] Here modes: T′ – lattice translation, δ – bending, δ_s – symmetric bending, δ_{as} – antisymmetric bending, ν_s – symmetric stretching, and ν_{as} – asymmetric.

Table 4 TO and LO vibration Raman A_1-spectra of the orthorhombic PbB_4O_7 crystal for two excitation geometries

with polished plane parallel faces. Two samples of orientation $[100]\times[010]\times[001]$ and $[100]\times[011]^e\times[0\bar{1}1]^e$, respectively, were used: sample 1: 10.26×7.00×6.34 mm^3; sample 2: 12.24×7.58×8.54 mm^3. Since the relatively small birefringence of PbB_4O_7 does not allow the realization of phase matching conditions for SHG the study of cascaded $\chi^{(2)} \leftrightarrow \chi^{(3)}$ processes is limited to non-phase-matched processes. It should be mentioned, however, that PbB_4O_7 possesses the highest SHG coefficients among the borate family (especially $d_{333}^{SHG} = 4.0(4)$ pm V^{-1} [10]). Some known physical properties of orthorhombic PbB_4O_7 single crystals are summarized in Table 2.

3. Stimulated and spontaneous Raman scattering

For the excitation of single-pass lasing Raman Stokes components in oriented orthorhombic non-centrosymmetric PbB_4O_7 single crystals we used a home-made Xe-flashlamp pumped picosecond Nd^{3+}:$Y_3Al_5O_{12}$ mode-locked laser with a two-pass Nd^{3+}:$Y_3Al_5O_{12}$ amplifier that can generate ≈ 110 ps pulses at $\lambda_f = 1.06415$ μm wavelength ($^4F_{3/2} \rightarrow {}^4I_{11/2}$ SE channel) (see, e.g. [2,20]). Its beam with nearly Gaussian profile is focused into the $(\chi^{(3)} + \chi^{(2)})$ active PbB_4O_7 samples with a lens ($f = 250$ mm), resulting in a beam-waist diameter of about 160 μm. The spectral composition of the nonlinear lasing emission in the visible and near-IR was investigated with a monochromator in Czerny-Turner arrangement (McPherson Model 270 with a grating of 150 lines/mm) and recorded by a spectrometric system with a Si-CCD array sensor (Hamamatsu S3923-1024Q with 1024 pixels). In the SRS experiments that were performed with different excitation orientations and with maximum possible pump power at $\lambda_f = 1.06415$ μm wavelength (up to optical damage threshold) for both samples multiple Stokes and anti-Stokes lasing component with equal energy spacing $\omega_{SRS} \approx 148$ cm^{-1} were observed. Due to $(\chi^{(3)} + \chi^{(2)})$ nonlinearity of the PbB_4O_7 crystal in addition to their multiple $\chi^{(3)}$-sidebands (which belong to the fundamental one-micron radiation) in the "green" spectral region a group of lines occurs in some pump geometries at proper pump power which are caused by cascaded $\chi^{(3)} \rightarrow \chi^{(2)}$ processes. These lines result from summing parametric interaction between pump and Stokes/anti-Stokes lasing photons ($\omega_{SRS} + \omega_{St/ASt}$). One of these spectra is shown in Fig. 4. Results of assignment of all recorded lines are listed in Table 3. It should be noted here that the observed SHG signal is not the result of a phase-matched process.

Since all SRS experiments were carried out under the steady-state (ss) pumping conditions $\tau_p \gg T_2 = (\pi \Delta\nu_R)^{-1} \approx 1.8$ ps (here T_2 is the phonon dephasing time and $\Delta\nu_R \approx 6$ cm^{-1} is the line width of the Raman shifted line related to the SRS-promoting vibration transition, see also Fig. 5), the corresponding Raman gain coefficient g_{ssR}^{St1} for the first Stokes generation at $\lambda_{St1} = 1.0812$ μm wavelength of the oriented PbB_4O_7 crystal could roughly be determined. For this estimation we referred to the sufficiently tested method (see, e.g. [21]) based on the well known ratio [22] $g_{ssR}^{St1} I_p^{thr} l_{SRS} \approx 30$ and a comparative measurement of the "threshold" pump intensity (I_p^{thr}) of the confidently detectable first-Stokes lasing signals of lead tetraborate and the reference crystal $PbWO_4$ ($\lambda_{St1} = 1.1770$ μm wavelength [23]) under similar excitation conditions. We found that the measured threshold for PbB_4O_7 is five to six times higher than that of the tungstate crystal. This results in a value of the g_{ssR}^{St1} coefficient not less than 0.5 cm GW^{-1}.

The orthorhombic (primitive) unit cell of the PbB_4O_7 crystal with space group symmetry C_{2v}^7 contains 24 atoms that have $3NZ = 72$ degrees of freedom (in Brillouin-zone center at $\mathbf{k} = 0$) described by the irreducible representation: Γ_{72} = 19A_1 + 17A_2 + 17B_1 + 19B_2. Among them A_1 + B_1 + B_2 are the acoustic modes; 7A_1 + 7A_2 + 6B_1 + 7B_2 are the lattice translational modes of the B^{3+} and

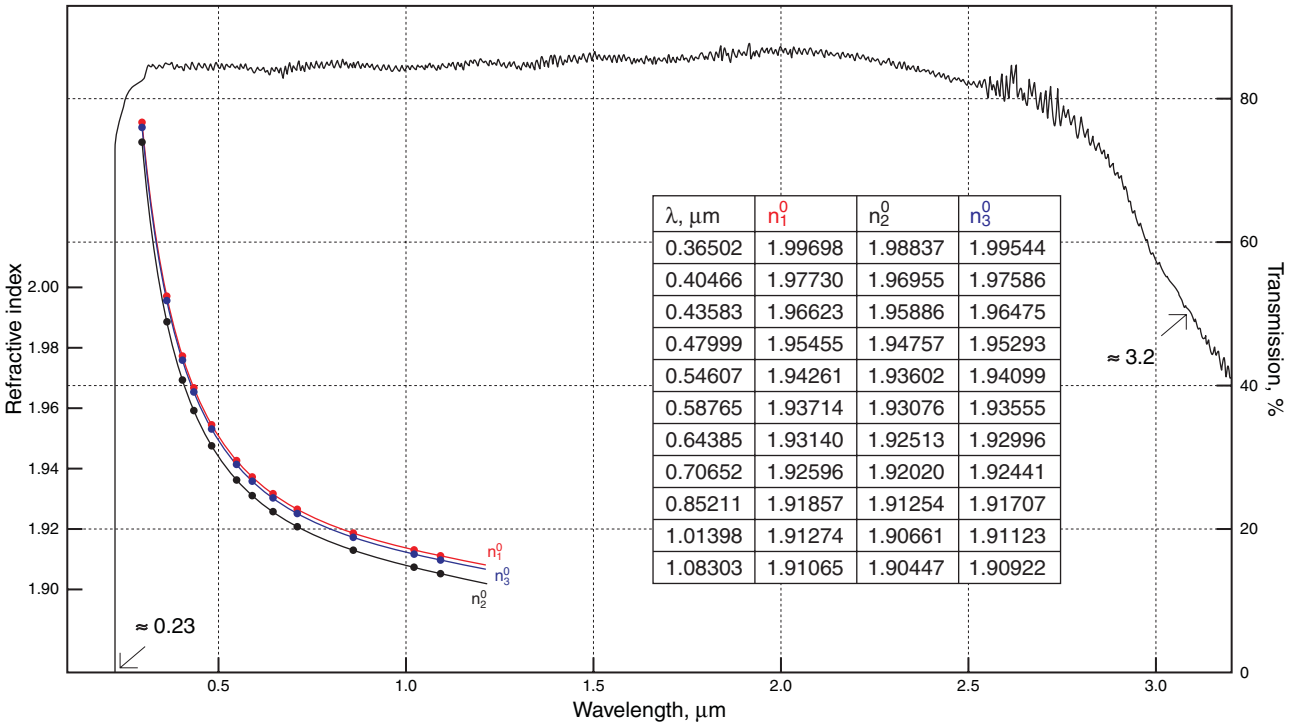

λ, µm	n_1^0	n_2^0	n_3^0
0.36502	1.99698	1.98837	1.99544
0.40466	1.97730	1.96955	1.97586
0.43583	1.96623	1.95886	1.96475
0.47999	1.95455	1.94757	1.95293
0.54607	1.94261	1.93602	1.94099
0.58765	1.93714	1.93076	1.93555
0.64385	1.93140	1.92513	1.92996
0.70652	1.92596	1.92020	1.92441
0.85211	1.91857	1.91254	1.91707
1.01398	1.91274	1.90661	1.91123
1.08303	1.91065	1.90447	1.90922

Figure 3 (online color at www.lphys.org) Room-temperature transmission spectrum in the range from UV to the mid-IR and wavelength dispersion of refractive indices (data from [10]) of an orthorhombic PbB_4O_7 single crystal

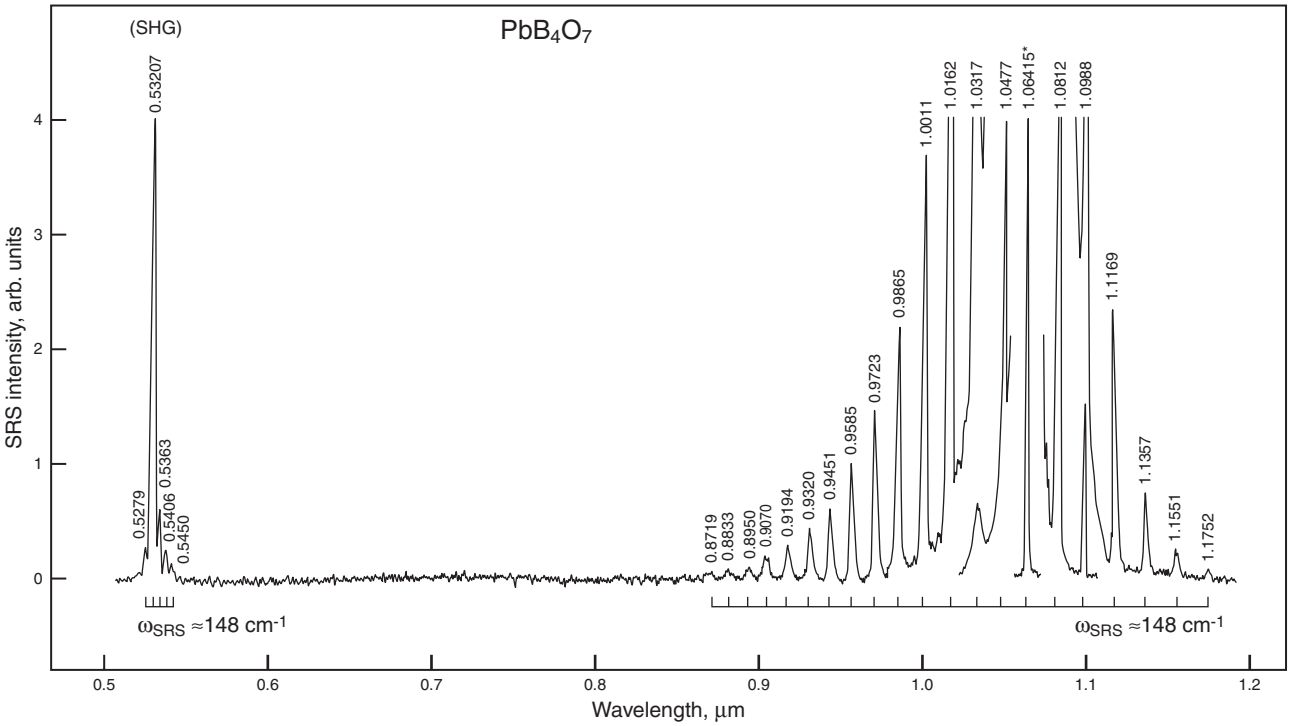

Figure 4 Room-temperature SRS, RFWM and cascaded $\chi^{(3)} \rightarrow \chi^{(2)}$ spectrum of a orthorhombic single crystal of PbB_4O_7 recorded in excitation geometry $c(qq)c$ (with $\mathbf{q} \parallel (\mathbf{e}_1 + \mathbf{e}_2)$) under pumping at $\lambda_f = 1.06415$ μm wavelength of Nd^{3+}:$Y_3Al_5O_{12}$ picosecond laser. $\chi^{(3)}$- and $\chi^{(2)}$- lasing lines related to the SRS-promoting vibration mode $\omega_{SRS} \approx 148$ cm^{-1} are indicated by horizontal brackets

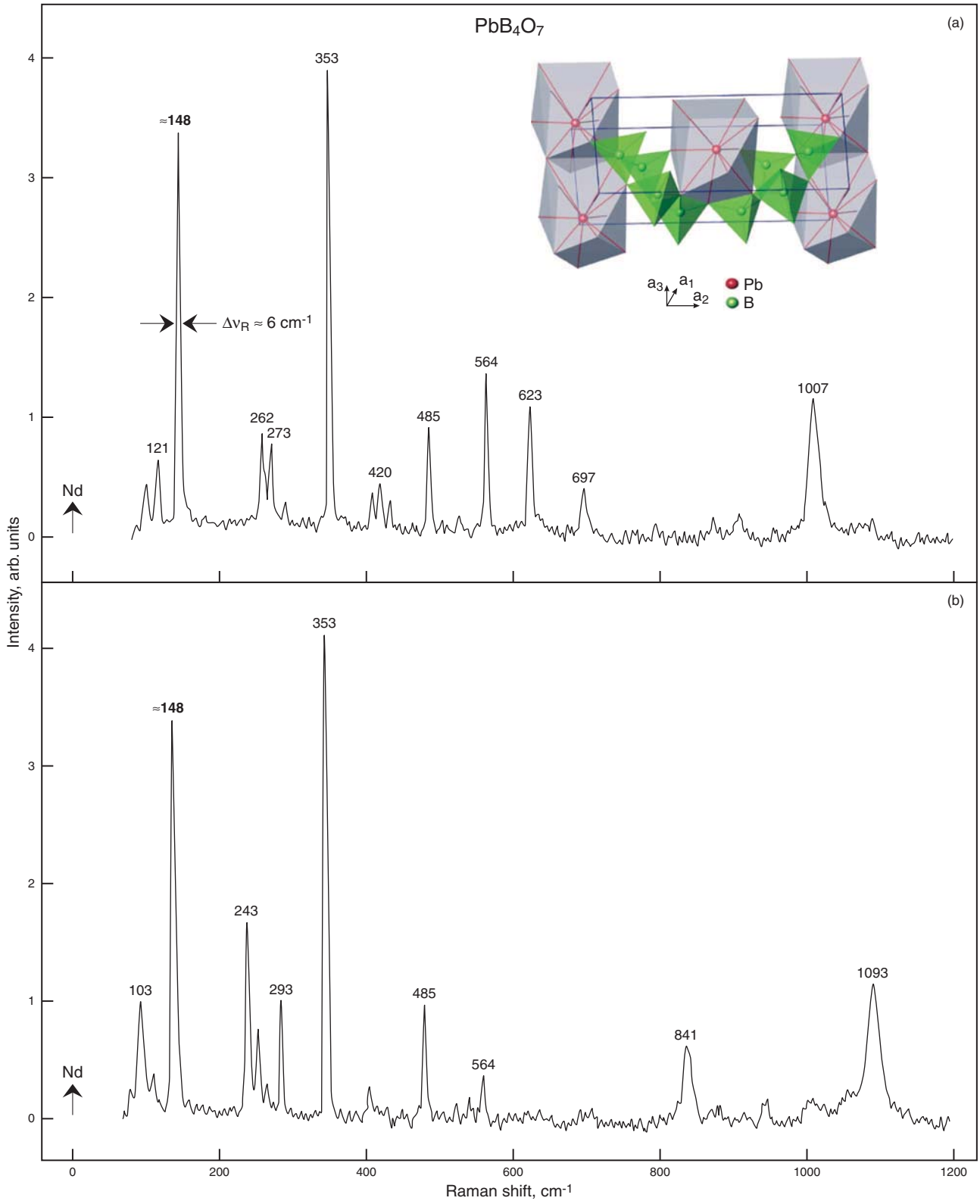

Figure 5 (online color at www.lphys.org) Room-temperature polarized spontaneous Raman scattering A_1-spectra of the orthorhombic PbB_4O_7 single crystal for two excitation geometries: (a) – *c(aa)c* and (b) – *c(bb)c*. The frequency of some Raman shifted lines are given in cm^{-1}. By arrows indicated excitation Nd^{3+}:$Y_3Al_5O_{12}$ laser line at 1.06415 μm wavelength. The inset in (a) presents a sketch of the unit cell of PbB_4O_7

Pb^{3+} ions; $11A_1$ + $10A_2$ + $10B_1$ + $11B_2$ are the internal modes involving the oxygen atoms. The A_1, B_1, and B_2 modes are IR- and Raman-active but A_2 modes are Raman-active only [24]. It means that A_1, B_1, and B_2 modes exhibit polar nature and TO-LO splitting could be determined from these spectra. From the full set of polarized Raman spectra (obtained using Bruker FT100/S spectrometer with CW one-micron Nd^{3+}:$Y_3Al_5O_{12}$ pumping laser) of an oriented PbB_4O_7 crystalline sample Fig. 5 shows two A_1-spectra which are recorded in excitation geometries that are close to the pumping condition used for the recording of the cascaded lasing ($\chi^{(3)} \rightarrow \chi^{(2)}$)-spectra spectra showed in Fig. 4. The wave numbers of the peaks of the two spectra of spontaneous Raman scattering with their tentative assignment to the respective normal modes are listed in Table 4.

Some features that can be concluded from the conducted Raman measurements are:

1) The lattice vibrations below 200 cm^{-1} correspond to the Pb^{2+} cations translation. Their energy is significantly lower than that of the corresponding vibrations of lithium and sodium tetraborates (see, e.g. [25]) where the lighter cations Li^+ and Na^+ appear. The translation of the significantly lighter B^{3+} cations contributes the vibration observed in the range 400–500 cm^{-1};
2) Among the modes observed in the A_1 Raman spectra (in Fig. 5 and as well in further spectra that are not presented here) the strongest lines at 353, $\approx$ 148, and 105 cm^{-1} could be $\chi^{(3)}$-promoting vibration modes. In our SRS experiments we observed $\omega_{SRS} \approx 148\ cm^{-1}$, only.

4. Conclusion

With the obtained results of nonlinear-laser and spectroscopic experiments on the SRS-active non-centrosymmetric PbB_4O_7 borate our knowledge on cascaded lasing $\chi^{(3)} \rightarrow \chi^{(2)}$ processes in nonlinear optical crystals is enhanced to a new structure type. The PbB_4O_7 crystal is of special interest for studies of cascaded $\chi^{(3)} \rightarrow \chi^{(2)}$ processes due to its rather high SHG coefficients with the lack of phase matching.

Acknowledgements The research reported here was performed within the "Joint Open Laboratory for Laser Crystals and Precise Laser Systems" and supported in part by the Russian Foundation for Basic Research and the Russian Academy of Sciences, as well as by the University of Cologne, the Technical University of Berlin, and the Institute of Low Temperature and Structure Research of the Polish Academy of Sciences. In his diploma thesis at the University of Cologne H. Roggendorf contributed to the development of the crystal growth of PbB_4O_7.

References

[1] P. Becker, Adv. Mater. **10**, 979 (1998).
[2] A.A. Kaminskii, L. Bohatý, P. Becker, J. Liebertz, H.J. Eichler, and H. Rhee, Laser Phys. Lett. **3**, 519 (2006).
[3] A. Perloff and S. Block, Acta Crystallogr. **20**, 274 (1966).
[4] J. Krogh-Moe, Acta Chem. Scand. **18**, 2055 (1964).
[5] K. Machida, G. Adachi, and J. Shiokawa, Acta Crystallogr. B **36**, 2008 (1980).
[6] H. Huppertz, Z. Naturforsch. **58b**, 257 (2003).
[7] H. Emme, M. Weil, and H. Huppertz, Z. Naturforsch. **60b**, 815 (2005).
[8] J.S. Knyrim, F.M. Schappacher, R. Pöttgen, J. Schmedt auf der Günne, D. Johrendt, and H. Huppertz, Chem. Mater. **19**, 254 (2007).
[9] L. Bohatý, Z. Kristallogr. **164**, 279 (1983).
[10] L. Bayarjargal, Lineare und nichtlineare optische Eigenschaften ausgewählter niedrigsymmetrischer Kristalle (PhD Dissertation, University of Cologne, 2006).
[11] D.L. Corker and A.M. Glazer, Acta Crystallogr. B **52**, 260 (1996).
[12] W.D. Stein, Struktur und Gitterdynamik in azentrischen Boraten (PhD Dissertation, University of Cologne, 2007).
[13] D.J. Liedberg, C.G. Ruderer, and C.G. Bergeron, J. Am. Ceram. Soc. **48**, 440 (1965).
[14] J. Liebertz, Prog. Crystal Growth Charact. **6**, 361 (1983).
[15] K.S. Bartwal, R. Bhatt, S. Kar, and V.K. Wadhawan, Mater. Sci. Eng. B **85**, 76 (2001).
[16] Yu.S. Oseledchik, A.L. Prosvirnin, A.I. Pisarevskiy, V.V. Starshenko, V.V. Osadchuk, S.P. Belokrys, N.V. Svitanko, A.S. Korol, S.A. Krikunov, and A.F. Selevich, Opt. Mater. **4**, 669 (1995).
[17] J.F.H. Nicholls, B.H.T. Chai, D. Russell, and B. Henderson, Opt. Mater. **8**, 185 (1997).
[18] H. Schneeberger, Pyroelektrische Eigenschaften nichtferroelektrischer Kristalle (PhD Dissertation, Ludwig-Maximilians-University, Munich, 1992).
[19] X.R. Zhang, Q.L. Zhang, Y.N. Lu, C.M. Gan, P.Z. Fu, H. Yin, and J.L. Zhou, Appl. Phys. A **66**, 351 (1998); Q. Zhou, S. Zhang, and Y. Lu, Mater. Sci. Eng. B **83**, 249 (2001).
[20] A.A. Kaminskii, L. Bohatý, P. Becker, H.J. Eichler, and R. Rhee, Laser Phys. Lett., **DOI** 10.1002/lapl.200710038.
[21] A.A. Kaminskii, H.J. Eichler, K. Ueda, N.V. Klassen, B.S. Redkin, L. Lu, J. Findeisen, D. Jaque, J. Garcia-Sole, J. Fernandez, and R. Balda, Appl. Opt. **38**, 4533 (1999).
[22] Y.R. Chen, The Principles of Nonlinear Optics (Wiley, New York, 1984).
[23] A.A. Kaminskii, C.L. McCray, H.R. Lee, S.W. Lee, D.A. Temple, T.H. Chyba, W.D. Marsh, J.C. Barnes, A.N. Annanenkov, V.D. Legun, H.J. Eichler, G.M.A. Gad, and K. Ueda, Opt. Commun. **183**, 277 (2000).
[24] D.L. Rousseau, R.P. Bauman, and S.P.S. Porto, J. Raman Spectrosc. **10**, 253 (1981).
[25] S.I. Furusawa, S. Tange, Y. Ishibashi, and K. Miwa, J. Phys. Soc. Japan **59**, 1825 (1990); Y. Li, and G. Lan, J. Phys. Chem. Solids **57**, 1887 (1996); M. Mączka, A. Waśkowska, A. Majchrowski, J. Żmija, J. Hanuza, G.A. Peterson and D.A. Keszler, J. Solid State Chem. **180**, 410 (2007).